CORRECTED 22 APRIL 2024; SEE FULL TEXT

Check for updates

PHYSICS

Parity violation in resonant inelastic soft x-ray scattering at entangled core holes

Johan Söderström[1]*, Anirudha Ghosh[2], Ludvig Kjellsson[2], Victor Ekholm[2], Takashi Tokushima[2], Conny Såthe[2], Nicolas Velasquez[3], Marc Simon[3], Olle Björneholm[1], Laurent Duda[1], Arnaldo Naves de Brito[4], Michael Odelius[5], Ji-Cai Liu[6,7], Jian Wang[6,8], Victor Kimberg[9], Marcus Agåker[1,2], Jan-Erik Rubensson[1], Faris Gel'mukhanov[9,10]

Copyright © 2024 The Authors, some rights reserved; exclusive licensee American Association for the Advancement of Science. No claim to original U.S. Government Works. Distributed under a Creative Commons Attribution NonCommercial License 4.0 (CC BY-NC).

Resonant inelastic x-ray scattering (RIXS) is a major method for investigation of electronic structure and dynamics, with applications ranging from basic atomic physics to materials science. In RIXS applied to inversion-symmetric systems, it has generally been accepted that strict parity selectivity applies in the sub–kilo–electron volt region. In contrast, we show that the parity selection rule is violated in the RIXS spectra of the free homonuclear diatomic O_2 molecule. By analyzing the spectral dependence on scattering angle, we demonstrate that the violation is due to the phase difference in coherent scattering at the two atomic sites, in analogy with Young's double-slit experiment. The result also implies that the interpretation of x-ray absorption spectra for inversion symmetric molecules in this energy range must be revised.

INTRODUCTION

Scattering, absorption, and emission of x-rays are central phenomena for our understanding of photon-matter interactions (*1*). While interference between x-rays scattered elastically at various sites provides the prime tool for unveiling the atomic geometry of matter (*2*), inner-shell transitions uncover its electronic structure (*3*).

Structural information is inherent in resonant inelastic x-ray scattering (RIXS) due to the interference between x-rays scattered at specific core hole sites, selected by tuning the incident energy to corresponding resonances. This implies that momentum conservation can be exploited (*4*) to map the dispersion of elementary excitations in crystals (*5*, *6*), and for a system with two scattering centers, interference in analogy with the canonical Young's double slit experiment (YDSE) has been predicted (*7*). This prediction was recently confirmed in the hard x-ray regime (*8*), and a new tool in solid-state physics termed RIXS interferometry is being established (*9*).

The prototypical system for investigation of YDSE interference in RIXS is a homonuclear diatomic molecule, where the photon can scatter at the two different atomic sites (*7*). Such systems have inversion symmetry, implying that the molecular wave function must have well-defined parity, either gerade or ungerade. In-phase scattering at the two atomic centers implies strict parity selectivity, so that only final states of the same parity as the initial state can be populated in the two-photon RIXS process. When the wavelength of the incident radiation is larger than the typical molecular dimensions, the in-phase requirement may appear fulfilled, and the validity of this molecular dipole approximation has generally been taken for granted in the soft x-ray range. For RIXS at short wavelengths, the in-phase requirement is only fulfilled in specific geometries, and consequently, the parity selection rule does not generally apply (*8*, *10*).

Nondipole effects are being investigated in photoionization (*11*), and notably, they have also been analyzed in terms of YDSE interference (*12*, *13*). In the strong field regime, effects beyond the dipole approximation now attract growing attention (*14*). So far, however, the parity selection rule has appeared to be strict in one-photon-in/one-photon-out soft x-ray RIXS (*15*–*17*). Here, we show that, while the atomic dipole approximation can still be safely applied in the soft x-ray range, the molecular dipole approximation cannot.

By measuring high-quality RIXS spectra of gas-phase O_2 as a function of scattering angle, using the rotatable spectrometer at the Veritas beamline at the MAX IV Laboratory, we demonstrate that parity selectivity is violated due to YDSE interference. Population of parity-forbidden final states is observed, and their dependence on the scattering angle is accurately reproduced by theory that analyzes the consequences of YDSE interference. Although the wavelength at the oxygen K edge ($\lambda \approx 23.5$ Å) is larger than the O_2 interatomic distance ($R \approx 1.21$ Å), the phase shift for scattering at the two centers is large enough to give the "dipole-forbidden" channel substantial intensity.

RESULTS

The experimental geometry is shown in Fig. 1. RIXS spectra of the free O_2 molecule, excited at the $1s \rightarrow \pi^*$ resonance and measured at scattering angles $\chi = 38°$, 90°, and 145°, are shown in Fig. 2A.

Energy losses in the 0- to 2-eV range are assigned to vibrational excitations in the $X\ ^3\Sigma_g^-$ electronic ground state with the configuration $1\sigma_g^2 1\sigma_u^2 2\sigma_g^2 2\sigma_u^2 3\sigma_g^2 1\pi_u^4 1\pi_g^2$, and energy losses in the 6.5- to 8.5-eV range are primarily due to population of the $B'\ ^3\Pi_g$ state, with the main configuration $3\sigma_g^{-1} 1\pi_g^{+1}$. This is in concordance with the results

[1]Department of Physics and Astronomy, Uppsala University, Box 516, SE-751 20, Uppsala, Sweden. [2]MAX IV Laboratory, Lund University, SE-221 00, Lund, Sweden. [3]Sorbonne Université, CNRS, UMR 7614, Laboratoire de Chimie Physique-Matiére et Rayonnement, F-75005 Paris, France. [4]Department of Applied Physics, Institute of Physics Gleb Wataghin Campinas University, CEP, Street, 13083859 Campinas SP, Brazil. [5]Department of Physics, Stockholm University, AlbaNova University Center, SE-106 91, Stockholm, Sweden. [6]School of Mathematics and Physics, North China Electric Power University, 102206 Beijing, China. [7]Hebei Key Laboratory of Physics and Energy Technology, North China Electric Power University, 071000 Baoding, China. [8]School of Nuclear Science and Technology, North China Electric Power University, 102206 Beijing, China. [9]Theoretical Chemistry and Biology, School of Biotechnology, Royal Institute of Technology, SE-106 91 Stockholm, Sweden. [10]Helmholtz Zentrum Berlin für Materialien und Energie, Institute for Methods and Instrumentation for Synchrotron Radiation Research, Albert-Einstein-Str. 15, D-12489 Berlin, Germany.
*Corresponding author. Email: johan.soderstrom@physics.uu.se

Downloaded from https://www.science.org at Uppsala University on February 04, 2025

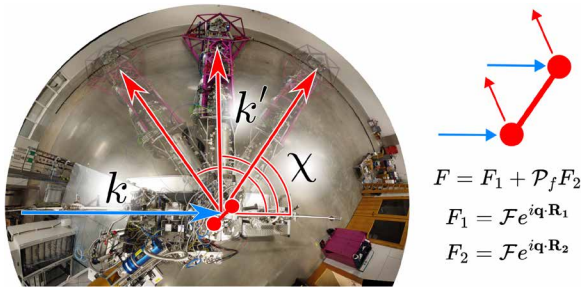

Fig. 1. Schematics of the experimental setup. Incident radiation with wave vector **k** is scattered at an angle χ. The wave vector of the scattered radiation is **k**′, and $\mathbf{q} = \mathbf{k}' - \mathbf{k}$. The variables are defined in wide-angle photo of the rotatable soft x-ray spectrometer at the Veritas beamline at MAX IV, which was used for the measurements. The essence of the theory is that scattering occurs at two identical atoms at the sites $\mathbf{R_1}$ and $\mathbf{R_2}$, with the same amplitude $\mathcal{F}$. The parity of the final state determines the sign of $\mathcal{P}_f = \pm 1$, see text for details.

and analysis of earlier investigations (*16*), as well as with parity selectivity: These final states have the same parity as the initial ground state.

Here, we turn our attention to the energy loss features in the 4- to 6.5-eV range. Sharp peaks are observed around 4.3 to 4.7 eV, followed by a broad structure toward larger energy losses with a maximum around 5.5 eV.

In Fig. 2B, the experimental spectrum measured at $\chi = 145°$ is analyzed using conventional Kramers-Heisenberg theory and Franck-Condon overlaps with potential curve parameters used earlier for the ground and intermediate states (*16*) and the parameters for the A′ $^3\Delta_u$, A $^3\Sigma_u^+$, and B $^3\Sigma_u^-$ final states from (*18*) (see the Supplementary Materials). The main configuration of these states is $1\pi_u^{-1}1\pi_g^{+1}$ (Fig. 2C). The agreement between the prediction and the experimental results allows for the conclusion that transitions to these parity-forbidden final states dominate the spectrum in the 3.95- to 6.35-eV energy region.

The intensity ratio of the forbidden ungerade to the allowed gerade final-state intensity is strongly dependent on the scattering angle, χ (Fig. 3). In the following, we will show that this angular dependence is in excellent agreement with a theory that analyzes interference in the same way as in a YDSE.

We consider the two equivalent atoms to have identical atomic amplitudes for photon scattering, $\mathcal{F} = (\mathbf{e}' \cdot \mathbf{d}')(\mathbf{e} \cdot \mathbf{d})$, where **e** and **e**′ are the polarization vectors of incoming and scattered photons, and **d** and **d**′ are the "atomic" transition dipole moments of the absorption and emission transitions (see the Supplementary Materials). The atomic dipole approximation is justified for core excitations in the soft x-ray regime, since the wavelength of the radiation is much larger than the extension of core orbitals for atoms with the nuclear charge $Z < 30$. Within this approximation, it can be shown that (see the Supplementary Materials) the combined scattering amplitude for two atoms with radius vectors $\mathbf{R_1}$ and $\mathbf{R_2}$ is (*7*) (see Fig. 1)

$$F = F_1 + F_2 = \mathcal{F}(e^{i\mathbf{q}\cdot\mathbf{R}_1} + \mathcal{P}_f e^{i\mathbf{q}\cdot\mathbf{R}_2}) \quad (1)$$

Here, $\mathbf{q} = \mathbf{k}' - \mathbf{k}$ is the difference between the wave vectors of the scattered, **k**′, and incident, **k**, photons, and $\mathcal{P}_f$ is the parity of the final state of the scattering process.

In RIXS, $\mathcal{P}_f = 1$ for parity-allowed gerade final states and $\mathcal{P}_f = -1$ for parity-forbidden ungerade final states. This theoretical result (Eq. 1) gives a clear physical picture: While the scattering is local at any of the atomic sites, the combined scattering amplitude is strongly dependent on the global inversion symmetry of the molecule. The process can be understood as scattering at entangled core-hole resonances at the two centra. The π difference in the phase shift of the electronic wave functions for ungerade and gerade final states results in a corresponding phase shift of the scattered radiation.

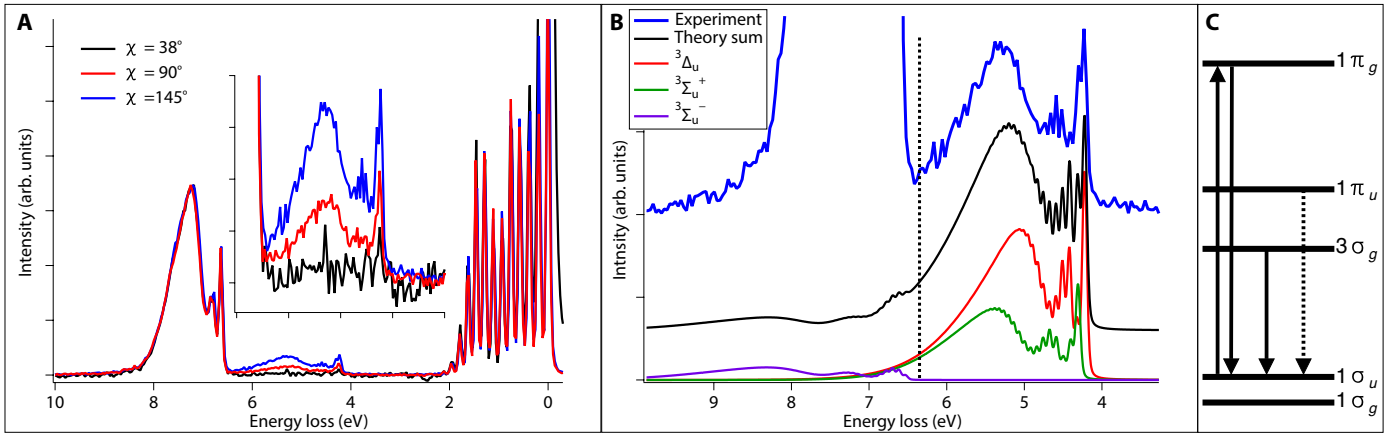

Fig. 2. Experimental and theoretical RIXS spectra excited at the π^* resonance of O_2. (**A**) RIXS spectra of the free O_2 molecule excited at the π^* resonance, measured at scattering angles $\chi = 38°$, 90°, and 145°. The spectra are normalized to the maximum of the peak around 7-eV energy loss. The inset shows a magnification of the intensity in the 4- to 6.4-eV energy range. (**B**) The spectrum in the 3- to 9-eV energy-loss region measured at $\chi = 145°$ is compared to a Franck-Condon analysis (see the Supplementary Materials) using the potential curves in (*18*) for the "parity-forbidden" A′ $^3\Delta_u$, A $^3\Sigma_u^+$, and B $^3\Sigma_u^-$ final states, derived from the $1\pi_u^{-1}1\pi_g^{+1}$ configuration. (**C**) A simplified level scheme showing the relevant transitions. Assuming strict parity selectivity an ungerade core hole opens when the electron is excited to a gerade orbital, and it is filled only by an electron from an orbital of the same (gerade) parity ("allowed" transitions, solid lines). Filling by an electron from an orbital of the opposite (ungerade) parity ("forbidden" transition, dashed line) implies violation of the molecular dipole selection rule.

Downloaded from https://www.science.org at Uppsala University on February 04, 2025

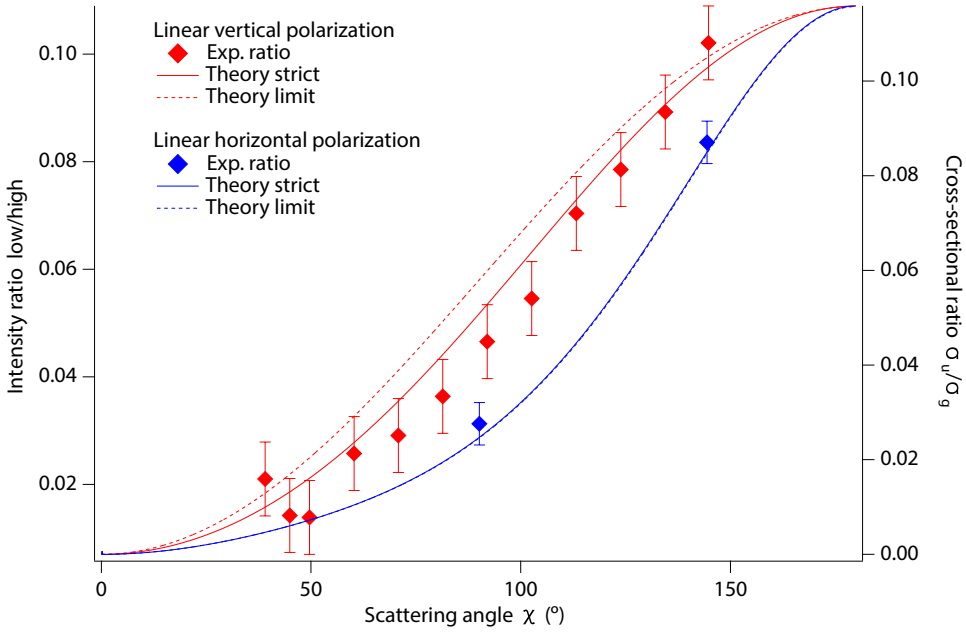

Fig. 3. Spectral dependence on scattering angle. The ratio of the intensity in the 3.95- to 6.35-eV region ("low") and the intensity in the 6.35- to 9.55-eV region ("high") as a function of the scattering angle χ. The separation between these two regions is indicated by a vertical dashed line in Fig. 2B. The experimental data are plotted using the scale of the left axis. Theoretical $\frac{\langle \sigma_u \rangle}{\langle \sigma_g \rangle}$, according to the strict expressions (solid line) and approximate expression (dashed line) in the limit of $2kR << 1$ are plotted using the scale of the right axis. The equations are derived in the Supplementary Materials, and we use the calculated $\zeta = \frac{d_u^2}{d_g^2} = 0.7$.

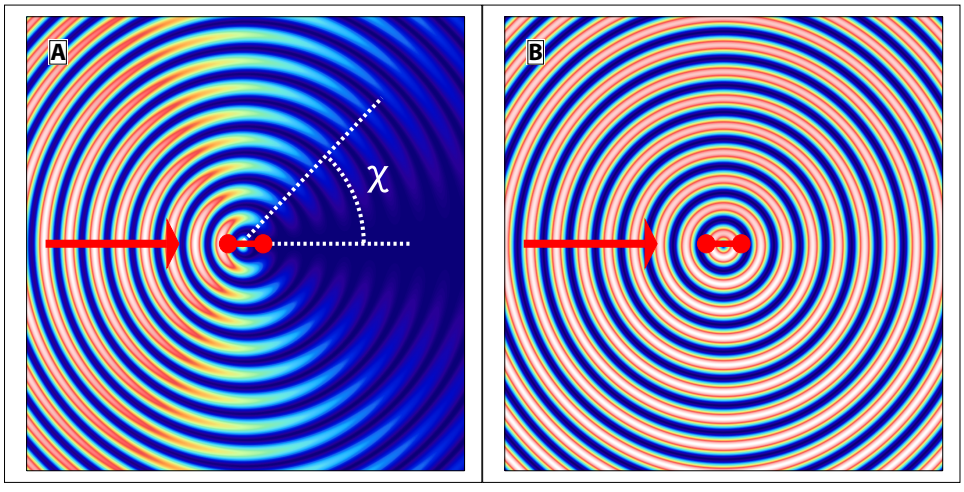

Fig. 4. Simulation of the scattered wave for a fixed-in-space molecule. (**A**) Scattering to ungerade final states and (**B**) scattering to gerade final states, assuming equal scattering amplitudes on both atomic sites. The intensity distribution is anisotropic for the ungerade final states and almost isotropic for the gerade final states. The incident radiation, indicated by a red arrow, enters from the left in the figure and scatters on the two atoms schematically shown as red circles. The molecular dimensions relative to the wavelength are not to scale. The wave amplitudes are normalized to the same maximum value in both figures.

As an illustration, we show a simplified two-dimensional simulation of the interference between waves from two point sources in Fig. 4. The sources correspond to scattering into gerade and ungerade final states from the two atomic scattering centers of a free fixed-in-space molecule. While scattering to allowed (gerade) final states implies no phase shift, scattering to forbidden (ungerade) final states implies a phase shift of π. The former case gives nearly isotropic scattering (Fig. 4B), whereas the latter gives a strong anisotropy (Fig. 4A): In forward scattering, the phase shift leads to destructive interference and negligible intensity, while additional phase shifts due to path length differences increase the scattered wave amplitude with increasing χ and give maximum intensity for backscattering.

Equation 1 is valid in the present case, as the splitting between the $1\sigma_g$ and $1\sigma_u$ core levels is small in comparison with the lifetime broadening of the core-excited state. A theory valid also for large *g*-*u* splitting will be published elsewhere. For a fixed-in-space molecule, Eq. 1 implies (see the Supplementary Materials) that the scattering cross section $\sigma_f = |F|^2$ takes the form

Downloaded from https://www.science.org at Uppsala University on February 04, 2025

$$\sigma_f = (dd')^2 \sigma_f^{\mathrm{dir}} \left[1 + \mathcal{P}_f \cos(\mathbf{q}\cdot\mathbf{R})\right] \quad (2)$$

where $\mathbf{R} = \mathbf{R_1} - \mathbf{R_2}$ is the interatomic radius vector, $\sigma_f^{\mathrm{dir}} = |(\mathbf{e}'\cdot\hat{\mathbf{d}}')(\mathbf{e}\cdot\hat{\mathbf{d}})|^2$ represents the cross section for independent scattering at one of the two equivalent sites, $\hat{\mathbf{d}} = \mathbf{d}/d$ and $\mathbf{d}' = \mathbf{d}'/d'$ are the unit vectors along the atomic dipole moment of the absorption and emission transitions, respectively. The cosine term in Eq. 2 describes the interference between scattering at the two centers in the same way as in YDSE. Strict parity selectivity requires $\mathbf{q}\cdot\mathbf{R} << 1$, so that $\cos(\mathbf{q}\cdot\mathbf{R}) \approx 1$ in Eq. 2. So far, it has been assumed that this requirement is fulfilled in the sub–kilo–electron volt region. Our results demonstrate, however, that this assumption is unjustified and that the spectral dependence on the scattering angle is due to YDSE interference.

RIXS spectra are measured as a function of scattering angle, χ. As only small energy losses are considered $k \approx k'$, and the relation between q and χ is given by simple geometry, $q = 2k \sin\frac{\chi}{2}$. Thus, while $q = 0$ in forward scattering ($\chi = 0$), it reaches maximum in backscattering ($\chi = \pi$). For scattering at the π* resonance of O_2, with 530-eV photon energy and 1.21-Å bond length, the maximum phase factor is $(qR)_{\max} \approx 0.65$. With $\mathbf{R}$ and $\mathbf{q}$ parallel, this gives $\cos(\mathbf{q}\cdot\mathbf{R}) \approx 0.8$, and a substantial deviation from strict parity selectivity is to be expected (Eq. 2).

For a quantitative comparison with RIXS measured on randomly oriented molecules, the cross section (Eq. 2) should be averaged over molecular orientations, $\hat{\mathbf{R}} = \mathbf{R}/R$

$$\langle\sigma_f\rangle = (dd')^2 \langle\sigma_f^{dir}\rangle (1 + \mathcal{P}_f \varrho_f), \varrho_f = \frac{\langle\sigma_f^{\mathrm{dir}} \cos(\mathbf{q}\cdot\mathbf{R})\rangle}{\langle\sigma_f^{\mathrm{dir}}\rangle} \quad (3)$$

The rather cumbersome derivation of the strict expressions for $\langle\sigma_f^{\mathrm{dir}}\rangle$ and ϱ_f is carried out in the Supplementary Materials. To get a qualitative picture of the physics behind the dependence of the interference term ρ_f on the scattering angle χ, we give a simplified expression for $\langle\sigma_f\rangle$ below. While YDSE interference for oriented molecules implies harmonic oscillations, $\cos(\mathbf{q}\cdot\mathbf{R})$ (Eq. 2), orientational dephasing dampens the oscillations at large qR. For randomly oriented molecules $\varrho_f \approx \langle\cos(\mathbf{q}\cdot\mathbf{R})\rangle = j_0(qR)$ (see eq. S28 in the Supplementary Materials), where $j_0(qR) = \frac{\sin(qR)}{qR}$ is the spherical Bessel function, and we get

$$\langle\sigma_f\rangle \propto d'^2\left[1 + \mathcal{P}_f j_0(qR)\right] = d'^2\left[1 + \mathcal{P}_f \frac{\sin(qR)}{qR}\right] \quad (4)$$

The ratio of the cross sections for scattering to parity-forbidden $\langle\sigma_u\rangle$ and parity-allowed $\langle\sigma_g\rangle$ final states is then

$$\frac{\langle\sigma_u\rangle}{\langle\sigma_g\rangle} \approx \frac{d_u^2}{d_g^2}\frac{\left[1 - j_0(qR)\right]}{\left[1 + j_0(qR)\right]} \quad (5)$$

where we also have introduced the transition dipole moments d_u and d_g for the emission step of the parity-forbidden and parity-allowed scattering, respectively, calculated without symmetry constraints. This simple equation, which is in qualitative agreement with the strict expressions, shows that the parity selection rules are violated due to YDSE interference in the soft x-ray region and that the selection rules are restored for forward scattering $\chi = 0°$, where $q = 0$.

In Fig. 3, we see that the theory (see eq. S29 in the Supplementary Materials) is in accordance with the experimental results. We conclude that interference of a photon scattered at two entangled core-hole sites is the principal mechanism behind parity selectivity as well as its violation.

DISCUSSION

For fixed-in-space or physisorbed molecules (*19*) and for two-center solids (*8*), YDSE interference, according to Eq. 2, remains important also in the hard x-ray regime ($qR >> 1$). For free molecules, however, orientational dephasing implies that the YDSE factor $j_0(qR) \rightarrow 0$ in Eq. 4 (except for $\chi \approx 0°$), and the RIXS process can be described as independent scattering at the two atomic centers, without parity selectivity. When $qR << 1$, as in forward scattering and at very long wavelengths, $j_0(qR) = 1$ implies strict parity selectivity for the RIXS process (Eq. 5). While it has earlier been assumed that this limit is reached in the soft x-ray regime, we have shown here that this is not the case.

We have described the phase difference for scattering at the two centers in terms of distance between the two scattering centers. The analysis can also be done in temporal terms, emphasizing the time difference between scattering at the two sites. Assuming that the photon travels at the speed of light in vacuum along the molecular axis, it reaches the second scattering center around 0.4 as after the first. This brings a small phase shift between RIXS channels via different centers and, hence, can affect parity selectivity related to scattering time differences in the zeptosecond regime. This is in line with the recent demonstration that the time delay between photoemission from the two centers of the hydrogen molecule can be resolved by interferometric methods (*20*).

Our analysis has consequences for the interpretation of x-ray absorption spectra (XAS). As the core electron is excited into an orbital of definite parity, it is often assumed that the parity of the core hole must be the opposite. However, the present analysis implies a contribution also from transitions that conserve parity, due to the phase difference $(\mathbf{k}\cdot\mathbf{R})$ for absorption at the two sites. The validity of this prediction is difficult to put to a direct experimental test because the split between allowed and forbidden excitations is due to the split between the core levels. This split is typically smaller than the lifetime broadening, and any contribution of the forbidden transition to the spectrum would be hard to discern. In RIXS, however, we have seen that final states of different parity can be well-separated. Therefore, this process can be used to monitor the minority absorption channel as a function of excitation energy (see fig. S2), and thus, the core-level *g*/*u* split between the $1\sigma_{g,u}^{-1}1\pi_g^{+1}$ states can be addressed in future experiments.

The present experiment is described by considering scattering at the sites of entangled local core holes, the entanglement being manifested in the parity-dependent phase shift at the two centers. In core-level spectroscopy in general, it has been recognized that it depends on the experimental arrangement whether the localized or the symmetric representation of the core hole is the most convenient (*6*, *21*). If the *g*/*u* split is neglected, like in the present analysis, then the two representations give equivalent results. While this is a safe approximation for O_2, where the split is small (*22*), it is not

Downloaded from https://www.science.org at Uppsala University on February 04, 2025

justified for a molecule like N_2 where the split is comparable to the lifetime width (*23*, *24*). Such a case calls for a more complex analysis than the one presented here.

In that situation, coherent core-hole wave packet dynamics can be addressed in RIXS by taking advantage of well-separated final states of opposite parity. It has also been proposed that this type of dynamics can be investigated in attosecond pump-probe experiments at x-ray free-electron lasers (*25*).

YDSE interference vanishes when which-path information is gained. In multiatom molecules, this can be caused by dynamic vibronic coupling (*26*–*28*), and for diatomics, an external disturbance may also break the symmetry. This is the case for adsorbed molecules (*29*), and recently, it has been demonstrated that protonation of N_2 molecules opens the XAS channel corresponding to parity-forbidden transitions in the symmetric molecule (*30*). Weak interactions between oxygen molecules and the surrounding are vital for numerous important processes, e.g., in reversible binding to metal complexes, which is essential in enzymatic and catalytic processes (*31*). The transport of O_2 via hemoglobin and blood plasma is fundamental to aerobic respiration, and lightly bound O_2 is also important in materials science (*32*) and electrochemistry (*33*). In the Supplementary Materials, we show how interaction with the asymmetric surrounding affects the relative intensity of the "symmetry-forbidden" band of O_2. YDSE interference can be important in the studied systems because the spacing between the 1s levels of inequivalent oxygen atoms is comparable to the large vibrational broadening of the core-excited state (~1 eV). In the near future, we plan to make a detailed investigation of the role of YDSE interference for the symmetry-forbidden channel in RIXS spectra of O_2 in condensed matter.

In conclusion, we have demonstrated that the parity selection rule implied by the molecular dipole approximation is violated in RIXS excited at the π^* resonance of gas-phase O_2. The spectral dependence on the scattering angle, measured at the Veritas beamline at MAX IV, is excellently described by a theory that considers YDSE interference.

METHODS

Experiment

The experiment was performed at the Veritas beamline at the MAX IV synchrotron radiation facility. The beamline comprises an elliptically polarizing undulator, a collimated plane-grating monochromator with an ellipsoidal refocusing mirror, and it is equipped with a large constant-line-spacing grating Rowland spectrometer (Fig. 1) with a collimating mirror in the nondispersive direction. The spectrometer can be continuously rotated in the horizontal plane to vary the scattering angle. We used a cylindrical grating with 1400 grooves/mm and 67 m radius and rotated the spectrometer to measure secondary radiation for scattering angles in the 38° to 145° range. The combined resolution for spectrometer and beamline was around 65 meV at the oxygen edge, as determined by the width of the elastic peak. Measurements were done both with linear horizontal and vertical polarization of the incident radiation. We used a cell with a 100-nm-thick Si_3N_4 membrane to separate the sample gas at atmospheric pressure from the ultrahigh vacuum of the surrounding. The incident and the emitted radiation penetrated the same membrane, in a geometry used in several earlier experiments, see, e.g., (*16*).

Simulations

The RIXS spectra were computed using the time-dependent wave packet approach (*19*, *34*) using the potential energy curves for the ground and core-excited from (*35*) and the core-excited lifetime width $\Gamma = 150$ meV (*16*). Morse constants for the final states are taken from the National Institute of Standards and Technology database, and details of the transition dipole moments calculations are explained in the Supplementary Materials. For the ungerade final states, we used the parameters from (*18*). See the Supplementary Materials for further details.

Supplementary Materials

This PDF file includes:

Supplementary Materials
Figs. S1 to S3
References

REFERENCES AND NOTES

1. J. Stöhr, Introduction and Overview, in *The Nature of X-Rays and Their Interactions with Matter*, Springer Tracts in Modern Physics, (Springer, Cham, ed. 1, 2023), vol. 288 pp. 1–55.
2. W. Friedrich, P. Knipping, M. Laue, Interferenzerscheinungen bei Röntgenstrahlen. *Ann. Phys.* **346**, 971–988 (1913).
3. H. G. J. Moseley, XCIII.The high-frequency spectra of the elements. *Lond. Edinb. Dublin Philos. Mag. J. Sci.* **26**, 1024–1034 (1913).
4. F. Gel'mukhanov, L. N. Mazalov, N. A. Shklyaeva, Some features of x-ray fluorescence in metals near the absorption threshold. *Zh. Eksp. Teor. Fiz.* **71**, 960–967 (1976).
5. L. J. P. Ament, M. van Veenendaal, T. P. Devereaux, J. P. Hill, J. van den Brink, Resonant inelastic x-ray scattering studies of elementary excitations. *Rev. Mod. Phys.* **83**, 705–767 (2011).
6. F. Gel'mukhanov, M. Odelius, S. P. Polyutov, A. Föhlisch, V. Kimberg, Dynamics of resonant x-ray and Auger scattering. *Rev. Mod. Phys.* **93**, 035001 (2021).
7. F. Gel'mukhanov, H. Ågren, Resonant inelastic x-ray scattering with symmetry-selective excitation. *Phys. Rev. A* **49**, 4378–4389 (1994).
8. A. Revelli, M. Moretti Sala, G. Monaco, P. Becker, L. Bohatý, M. Hermanns, T. C. Koethe, T. Fröhlich, P. Warzanowski, T. Lorenz, S. V. Streltsov, P. H. M. van Loosdrecht, D. I. Khomskii, J. van den Brink, M. Grüninger, Resonant inelastic x-ray incarnation of Young's double-slit experiment. *Sci. Adv.* **5**, eaav4020 (2019).
9. M. Magnaterra, M. Moretti Sala, G. Monaco, P. Becker, M. Hermanns, P. Warzanowski, T. Lorenz, D. I. Khomskii, P. H. M. van Loosdrecht, J. van den Brink, M. Grüninger, RIXS interferometry and the role of disorder in the quantum magnet $Ba_3Ti_{3-x}Ir_xO_9$. *Phys. Rev. Res.* **5**, 013167 (2023).
10. J. D. Mills, J. A. Sheehy, T. A. Ferrett, S. H. Southworth, R. Mayer, D. W. Lindle, P. W. Langhoff, Nondipole resonant x-ray raman spectroscopy: Polarized inelastic scattering at the *K* Edge of Cl_2. *Phys. Rev. Lett.* **79**, 383–386 (1997).
11. I. E. Brumboiu, O. Eriksson, P. Norman, Photoelectron spectroscopy of molecules beyond the electric dipole approximation. *J. Chem. Theory Comput.* **15**, 5483–5494 (2019).
12. X.-J. Liu, Q. Miao, F. Gel'mukhanov, M. Patanen, O. Travnikova, C. Nicolas, H. Ågren, K. Ueda, C. Miron, Einstein–Bohr recoiling double-slit gedanken experiment performed at the molecular level. *Nat. Photonics* **9**, 120–125 (2015).
13. S. E. Canton, E. Plésiat, J. D. Bozek, B. S. Rude, P. Decleva, F. Martín, Direct observation of Young's double-slit interferences in vibrationally resolved photoionization of diatomic molecules. *Proc. Natl. Acad. Sci. U.S.A.* **108**, 7302–7306 (2011).
14. R. Kahvedžić, S. Gräfe, Strong-field approximation with leading-order nondipole corrections. *Phys. Rev. A* **105**, 063102 (2022).
15. P. Glans, K. Gunnelin, P. Skytt, J.-H. Guo, N. Wassdahl, J. Nordgren, H. Ågren, F. K. Gel'mukhanov, T. Warwick, E. Rotenberg, Resonant x-ray emission spectroscopy of molecular oxygen. *Phys. Rev. Lett.* **76**, 2448–2451 (1996).
16. F. Hennies, A. Pietzsch, M. Berglund, A. Föhlisch, T. Schmitt, V. Strocov, H. O. Karlsson, J. Andersson, J.-E. Rubensson, Resonant inelastic scattering spectra of free molecules with vibrational resolution. *Phys. Rev. Lett.* **104**, 193002 (2010).
17. J. Söderström, R. Stefanuik, F. Hennies, T. Schmitt, V. N. Strocov, J. Andersson, B. Kennedy, J. Schlappa, A. Föhlisch, A. Pietzsch, J.-E. Rubensson, Resonant inelastic x-ray scattering on CO_2: Parity conservation in inversion-symmetric polyatomics. *Phys. Rev. A* **101**, 062501 (2020).
18. K. P. Huber, G. Herzberg, Constants of diatomic molecules, in *Molecular structure and molecular spectra, Vol. 4. Constants of diatomic molecules*. Van Nostrand Reinhold, New York, (1979).

Downloaded from https://www.science.org at Uppsala University on February 04, 2025

19. F. Gel'mukhanov, H. Ågren, Resonant x-ray raman scattering. *Phys. Rep.* **312**, 87–330 (1999).
20. S. Grundmann, D. Trabert, K. Fehre, N. Strenger, A. Pier, L. Kaiser, M. Kircher, M. Weller, S. Eckart, L. P. H. Schmidt, F. Trinter, T. Jahnke, M. S. Schöffler, R. Dörner, Zeptosecond birth time delay in molecular photoionization. *Science* **370**, 339–341 (2020).
21. M. S. Schöffler, J. Titze, N. Petridis, T. Jahnke, K. Cole, L. P. H. Schmidt, A. Czasch, D. Akoury, O. Jagutzki, J. B. Williams, N. A. Cherepkov, S. K. Semenov, C. W. McCurdy, T. N. Rescigno, C. L. Cocke, T. Osipov, S. Lee, M. H. Prior, A. Belkacem, A. L. Landers, H. Schmidt-Böcking, T. Weber, R. Dörner, Ultrafast probing of core hole localization in N_2. *Science* **320**, 920–923 (2008).
22. S. L. Sorensen, K. J. Børve, R. Feifel, A. de Fanis, K. Ueda, The O 1s photoelectron spectrum of molecular oxygen revisited. *J. Phys. B* **41**, 095101 (2008).
23. U. Hergenhahn, O. Kugeler, A. Rüdel, E. E. Rennie, A. M. Bradshaw, Symmetry-selective observation of the N 1s shape resonance in N_2. *J. Phys. Chem. A* **105**, 5704–5708 (2001).
24. M. Alagia, R. Richter, S. Stranges, M. Agåker, M. Ström, J. Söderström, C. Såthe, R. Feifel, S. Sorensen, A. De Fanis, K. Ueda, R. Fink, J.-E. Rubensson, Core level ionization dynamics in small molecules studied by x-ray-emission threshold-electron coincidence spectroscopy. *Phys. Rev. A* **71**, 012506 (2005).
25. L. Inhester, L. Greenman, A. Rudenko, D. Rolles, R. Santra, Detecting coherent core-hole wave-packet dynamics in N_2 by time- and angle-resolved inner-shell photoelectron spectroscopy. *J. Chem. Phys.* **151**, 054107 (2019).
26. P. Skytt, P. Glans, J.-H. Guo, K. Gunnelin, C. Såthe, J. Nordgren, F. K. Gel'mukhanov, A. Cesar, H. Ågren, Quenching of symmetry breaking in resonant inelastic x-ray scattering by detuned excitation. *Phys. Rev. Lett.* **77**, 5035–5038 (1996).
27. C. Miron, V. Kimberg, P. Morin, C. Nicolas, N. Kosugi, S. Gavrilyuk, F. Gel'mukhanov, Vibrational scattering anisotropy generated by multichannel quantum interference. *Phys. Rev. Lett.* **105**, 093002 (2010).
28. T. Marchenko, S. Carniato, L. Journel, R. Guillemin, E. Kawerk, M. Žitnik, M. Kavčič, K. Bučar, R. Bohinc, M. Petric, V. Vaz da Cruz, F. Gel'mukhanov, M. Simon, Electron dynamics in the core-excited CS_2 Molecule revealed through resonant inelastic x-ray scattering spectroscopy. *Phys. Rev. X* **5**, 031021 (2015).
29. A. Nilsson, L. G. M. Pettersson, Chemical bonding on surfaces probed by X-ray emission spectroscopy and density functional theory. *Surf. Sci. Rep.* **55**, 49–167 (2004).
30. R. C. Couto, W. Hua, R. Lindblad, L. Kjellsson, S. L. Sorensen, M. Kubin, C. Bülow, M. Timm, V. Zamudio-Bayer, B. von Issendorff, J. Söderström, J. T. Lau, J.-E. Rubensson, H. Ågren, V. Carravetta, Breaking inversion symmetry by protonation: Experimental and theoretical NEXAFS study of the diazynium ion, N_2H^+. *Phys. Chem. Chem. Phys.* **23**, 17166–17176 (2021).
31. D. Jeong, J. Selverstone Valentine, J. Cho, Bio-inspired mononuclear nonheme metal peroxo complexes: Synthesis, structures and mechanistic studies toward understanding enzymatic reactions. *Coord. Chem. Rev.* **480**, 215021 (2023).
32. C. Århammar, A. Pietzsch, N. Bock, E. Holmström, C. Moyses Araujo, J. Gråsjö, S. Zhao, S. Green, T. Peery, F. Hennies, S. Amerioun, A. Föhlisch, J. Schlappa, T. Schmitt, V. N. Strocov, G. A. Niklasson, D. C. Wallace, J.-E. Rubensson, B. Johansson, R. Ahuja, Unveiling the complex electronic structure of amorphous metal oxides. *Proc. Natl. Acad. Sci. U.S.A.* **108**, 6355–6360 (2011).
33. R. A. House, U. Maitra, M. A. Pérez-Osorio, J. G. Lozano, L. Jin, J. W. Somerville, L. C. Duda, A. Nag, A. Walters, K.-J. Zhou, M. R. Roberts, P. G. Bruce, Superstructure control of first-cycle voltage hysteresis in oxygen-redox cathodes. *Nature* **577**, 502–508 (2020).
34. P. Sałek, F. Gel'mukhanov, H. Ågren, Wave-packet dynamics of resonant x-ray Raman scattering: Excitation near the Cl $L_{II,III}$ edge of HCl. *Phys. Rev. A* **59**, 1147–1159 (1999).
35. M. Coreno, M. De Simone, K. C. Prince, R. Richter, M. Vondráček, L. Avaldi, R. Camilloni, Vibrationally resolved oxygen K $\rightarrow \Pi^*$ spectra of O_2 and CO. *Chem. Phys. Lett.* **306**, 269–274 (1999).
36. J. Söderström, Data for figures in the paper "Parity violation in resonant inelastic soft x-ray scattering at entangled core holes", 10.5281/zenodo.10068862 (2023).
37. V. K. Khersonskii, A. N. Moskalev, D. A. Varshalovich, *Quantum Theory Of Angular Momentum*. World Scientific Publishing Company (1988).
38. I. F. Galván, M. Vacher, A. Alavi, C. Angeli, F. Aquilante, J. Autschbach, J. J. Bao, S. I. Bokarev, N. A. Bogdanov, R. K. Carlson, L. F. Chibotaru, J. Creutzberg, N. Dattani, M. G. Delcey, S. S. Dong, A. Dreuw, L. Freitag, L. M. Frutos, L. Gagliardi, F. Gendron, A. Giussani, L. González, G. Grell, M. Guo, C. E. Hoyer, M. Johansson, S. Keller, S. Knecht, G. Kovačević, E. Källman, G. L. Manni, M. Lundberg, Y. Ma, S. Mai, J. P. Malhado, P. Å. Malmqvist, P. Marquetand, S. A. Mewes, J. Norell, M. Olivucci, M. Oppel, Q. M. Phung, K. Pierloot, F. Plasser, M. Reiher, A. M. Sand, I. Schapiro, P. Sharma, C. J. Stein, L. K. Sørensen, D. G. Truhlar, M. Ugandi, L. Ungur, A. Valentini, S. Vancoillie, V. Veryazov, O. Weser, T. A. Wesołowski, P.-O. Widmark, S. Wouters, A. Zech, J. P. Zobel, R. Lindh, OpenMolcas: From source code to insight. *J. Chem. Theory Comput.* **15**, 5925–5964 (2019).
39. B. O. Roos, R. Lindh, P.-Å. Malmqvist, V. Veryazov, P.-O. Widmark, Main group atoms and dimers studied with a new relativistic ANO basis set. *J. Phys. Chem. A* **108**, 2851–2858 (2004).
40. M. Guo, L. K. Sørensen, M. G. Delcey, R. V. Pinjari, M. Lundberg, Simulations of iron K pre-edge X-ray absorption spectra using the restricted active space method. *Phys. Chem. Chem. Phys.* **18**, 3250–3259 (2016).

Acknowledgments: We would like to thank the staff of MAX IV Laboratory for a smooth operation of the synchrotron during the experiment. **Funding:** J.-E.R. acknowledges funding from the Swedish Research Council (no. 2021-04017). L.D. acknowledges financial support from the Swedish Energy Agency to the project "x-ray based methodology for next generation Na-ion battery cathodes" (project number: 50745-1). M.A. acknowledges the Swedish Foundation for Strategic Research (grant RIF14-0064). M.O. acknowledges funding from the Swedish Research Council (no. 2021-04521). N.V. acknowledges funding from the European Research Council Horizon 2020 research and innovation program under Marie Skłodowska-Curie (grant agreement no. 860553). V.K. acknowledges funding from the Swedish Research Council (no. 2019-03470). J.-C.L. acknowledges financial support from National Natural Science Foundation of China (nos. 11974108 and 12211530044). Computations were enabled by resources provided by the National Academic Infrastructure for Supercomputing in Sweden (NAISS) and the Swedish National Infrastructure for Computing (SNIC), partially funded by the Swedish Research Council through grant agreement nos. 2022-06725 and 2018-05973. A.N.B. acknowledges support from FAPESP (grant number 2017/11986-5), the R and D levy regulation, National Council for Scientific and Technological Development CNPq 401581/2016-0, and STINT-CAPES (grants nos. 9805/2014-01 and 88881.465527/2019-01). **Author contributions:** Conceptualization: V.E., J.S., F.G., A.G., A.N.B., O.B., J.-E.R., C.S., and L.D.. Data curation: V.E., J.S., L.K., and V.K. Formal analysis: V.E., J.S., L.K., A.G., M.O., J.-C.L., V.K., and L.D. Funding acquisition: J.-E.R., V.K., and L.D. Investigation: N.V., V.E., F.G., M.S., A.G., M.A., A.N.B., O.B., J.-E.R., M.O., T.T., and C.S. Methodology: V.E., J.S., L.K., F.G., M.A., O.B., J.-E.R., T.T., V.K., C.S., and L.D. Project administration: A.G., M.A., J.-E.R., and C.S. Resources: V.E., A.G., J.-C.L., and C.S. Software: V.E., J.S., L.K., A.G., J.-C.L., and V.K. Supervision: A.G., A.N.B., J.-E.R., and C.S. Validation: J.S., F.G., M.S., O.B., J.-E.R., J.-C.L., T.T., V.K., J.W., C.S., and L.D. Visualization: J.S., L.K., A.N.B., J.-E.R., J.-C.L., V.K., and L.D. Writing—original draft: J.S., F.G., J.-E.R., and L.D. Writing—review and editing: J.S., F.G., M.S., A.N.B., O.B., J.-E.R., J.-C.L., and L.D. **Competing interests:** The authors declare that they have no competing interests. **Data and materials availability:** All data needed to evaluate the conclusions in the paper are present in the paper and/or the Supplementary Materials. All data used to generate the figures in this paper is available in (*36*) (https://zenodo.org/doi/10.5281/zenodo.10068861).

Submitted 14 August 2023
Accepted 12 January 2024
Published 14 February 2024
10.1126/sciadv.adk3114

Downloaded from https://www.science.org at Uppsala University on February 04, 2025